J Nanopart Res (2010) 12:2335–2347
DOI 10.1007/s11051-010-9939-9

PERSPECTIVES

Highly conductive polymers: superconductivity in nanochannels or an experimental artifact?

Harley Hayden · Seongho Park · Victor Zhirnov · Ralph Cavin · Paul A. Kohl

Received: 7 January 2010 / Accepted: 16 April 2010 / Published online: 1 May 2010
© Springer Science+Business Media B.V. 2010

Abstract There is a significant body of literature concerning the potential formation of electrically conductive moieties in polymeric materials. The conductive path is not associated with conjugation (such as in the case of 'conductive polymers') but rather associated with a new conductivity route. The objective of the experiments reported herein was to provide insight into the phenomenon of unusually high electrical conductivity in polymers that have been reported by several research groups. In some experiments, the test apparatus did indeed indicate high levels of conductance. Arguments pro and con for high conductivity based on known physical phenomena and the collected data were examined.

Keywords Conductive polymers · High-temperature superconductivity · Constriction resistance · Modeling and simulation

H. Hayden · S. Park · P. A. Kohl
School of Chemical and Biomolecular Engineering, Georgia Institute of Technology, Atlanta, GA 30332-0100, USA

V. Zhirnov (✉) · R. Cavin
Semiconductor Research Corporation, Research Triangle Park, Durham, NC 27709-2053, USA
e-mail: zhirnov@src.org

Introduction

In the scientific literature, there has appeared a series of papers that suggest that certain polymers, which are normally insulators, sometimes offer very high electrical conductivity. In this paper, we refer to these materials as highly conductive polymers (HCP). Indeed, these reports are not without controversy since some researchers counter that the observed data could be explained by experimental artifacts, such as by the formation of metal-like filaments between metal electrodes. This paper reports on our efforts to experimentally verify the claimed occurrences of high conductivity in polymers and to comprehend a physical basis for the phenomena, if it could be demonstrated.

There is a significant body of literature on the topic of HCP and several of the most representative publications are reviewed here. In 1989, a group from the Institute of Synthetic Polymeric Materials, Moscow, Russia reported on very low electrical resistivity for a thin polymer film in the direction normal to the surface (Enikolopyan et al. 1989). The work was reproduced by a group in Ioffe Physico-Technical Institute, St. Petersburg, Russia, which conducted experiments both at room temperature and cryogenic (to achieve a superconducting state on metal electrodes) temperatures (Ionov et al. 2005, 2007).

In 1992, a group at the Ioffe Institute concluded that the low-resistance state was due to *metallic*

bridge formation from electrode material (Ionov et al. 1992). An additional study from Bar-Ilan University, Israel in 1998 was conducted "to verify whether or not the low-resistance state in the above experiments can be explained by the formation either metallic or carbon bridge between the contacts" (Shlimak and Martchenkov 1998). In their experiments with poly-dimethylsiloxane (PDMS), two switching regimes were found. The first regime is at high switching voltage and the second is at low voltage. If the applied voltage exceeded some threshold value $V_{th} > 100$ V, the sample resistance switched from the normal high-resistance state ($R \sim 10^9$ Ohm) to the low-resistance state with typical resistance of a few Ohms. The formation of a metal bridge from the metallic electrodes (copper in their case) was clearly observed. In the high-voltage regime, the maximum current in the low-resistance state was $I_{max} < 100$ mA and it was limited by melting of the metal bridge.

In the low-voltage switching (LVS) regime, the voltage applied to the polymer films did not exceed 1 V, which is smaller than the electrical breakdown in the previous, high-voltage switching regime. The polymer films were 5–12 μm thick and the resistance was observed to switch randomly between the high-resistance OFF state (about 10^9 Ohm) and the low-resistance ON state (about 0.4–0.5 Ohm). The ON state remained after the voltage was terminated showing a memory effect. However, the conductivity disappeared and reappeared spontaneously. The switching from the high-to-low resistance state occurred after ~8 to 10 h of low-voltage biasing. For thicker films (thickness >15 μm), the ON state was not observed even after several days of observation.

The ON state of the polymer had particular characteristics. First, the sample resistance in the ON state did not depend on the cross sectional area of the polymer film between the electrodes. The sample area in these experiments varied from 0.1 to 0.4 cm^2. Second, the most intriguing property of the LVS ON state is its high current, which exceeded 2 A for several hours in a parallel-plate configuration without damage. The maximum current was limited by metallic electrode failure. The current–voltage (*I–V)* curve in the LVS ON state was linear up to the maximal current, which may suggest that there is little temperature rise or that the resistivity is temperature independent. Finally, the resistance of the 'Ultra-Switching' ON state was $R = 0.4$–0.5 Ohm, which can be attributed either to the polymer film itself or to the contact between the film and metal electrode: $R_{ON} = R_{film} + R_{cont}$. The authors concluded that the low-voltage switching is a new effect, which can not be explained in terms of conventional dielectric breakdown.

This investigation endeavors to examine the low-resistance state observed in the literature while controlling for possible non-polymer conduction pathways. These pathways include electrode–electrode shorting, metal filament formation, and carbon filament formation. A combination of experimental observation and theoretical treatment of each possible conduction mechanism is utilized to enhance the current understanding of these phenomena.

Description of experiments

In an effort to test whether or not specific electrically insulating polymers can become highly conductive, three materials were investigated: Sylgard 184 polydimethylsiloxane (PDMS-1) purchased from Dow Corning Corporation, a second polydimethylsiloxane material (PDMS-2) with MW = 170,300 purchased from Aldrich Chemical, and poly(*n*-octyl methacrylate) (POMA) with a MW of 100,000 purchased from Scientific Polymer Products Inc. The PDMS materials were used in pure form, without solvent, whereas the POMA was obtained as a 25.23 wt% mixture in toluene. The polymer materials were placed on an electrode surface drop-wise, with an excess amount of polymer dispensed to ensure electrode coverage. The polymers were not cured during the treatment process. In a number of previous works (e.g., Rogachev and Grigorov 2000), it was suggested that UV treatment of polymer films increases the likelihood of switching from insulating to the highly conductive state. In this work, the polymer was exposed to 365 nm wavelength radiation at an intensity of 42 mW/cm^2 for 60 min for a total dose of 150 J/cm^2. Samples were allowed to cool to room temperature following exposure before testing was initiated.

In order to apply a voltage across the polymer materials two different test structures were used, parallel-plate capacitors and comb electrodes. The

parallel-plate capacitors were fabricated by depositing a metal film on a 4 inch diameter quartz or oxidized silicon wafer substrate. The wafers were approximately 0.5 mm thick. The bottom electrode was patterned into nine electrically isolated metal capacitor pads that were 10 × 10 mm square. A schematic of the bottom electrode is shown in Fig. 1. Each of the metal squares was connected to a metal pad which could be electrically probed. The metal lines connecting the electrode squares to the probe pads were 1.5 mm wide traces and the length varied between 1.5 and 5 cm long The metal pattern on the bottom electrode was fabricated by sputtering 10 nm of titanium (for adhesion) followed by 500 nm of gold or chromium over the whole wafer. Photoresist was used to cover the metal squares, probe pads, and connecting lines. The exposed, unwanted metal was chemically etched. The top electrode was composed of a rectangular oxidized silicon wafer with 10 nm of titanium (for adhesion) followed by 500 nm of gold or 500 nm of chromium across the entire surface. The top electrode was positioned over the bottom electrode as shown in Fig. 1. This electrode was secured with weights and tape to eliminate any movement and ensure good contact between the polymer and the electrode surfaces. The top plate was large enough to completely cover the capacitor squares on the bottom electrode but not the probe pads. The top wafer extended over the edge of the bottom substrate for easy electrical contact.

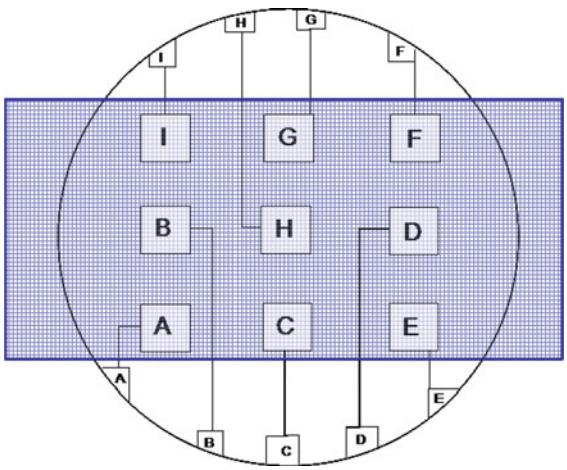

Fig. 1 *Bottom* (*round* wafer) and *top* (*rectangular*, *blue*) electrode set-up

Since the dielectric materials were viscous fluids, it was necessary to rigidly fix the gap between the two electrode plates in this configuration in order to avoid direct contact between electrodes and an electrically closed circuit. Three distinct gap control methods (GCM) were used for the parallel-plate electrodes. The first method (GCM-1) used a 1 μm thick layer of deposited silicon dioxide that was lithographically patterned into 5 × 5 mm openings on the 10 × 10 mm metal pad. The thickness of the silicon dioxide spacer was measured with a profilometer and was found to be 1–1.5 μm thick. The silicon dioxide was deposited by plasma enhanced chemical vapor deposition. The electrode assembly was completed by placing the top electrode plate, as shown in Fig. 1, over the bottom silicon electrode structure, resulting in the structure shown in Fig. 2.

The second approach (GCM-2) to controlling the spacing between top and bottom electrodes used silica spacers between the parallel electrode plates. Silica spheres, each 1 μm in diameter, were placed on the bottom electrode followed by dispensing of the liquid dielectric material. The particles were dispensed with a needle tip in two configurations. The first method dispensed the particles at the four corners of the electrode pad and along the length of the lines connecting the electrode pad to the contact pads along the edge of the wafer (GCM-2a)The second method added an additional droplet of spacers in the center of the electrode pad (GCM-2b). The spacer configuration leaves the entire 10 × 10 mm electrode pad open for conduction (1 cm^2). The actual gap between the electrodes in these cases likely ranged from 3 to 6 μm due to particle stacking and agglomeration based on SEM images of the particles after processing (Fig. 3).

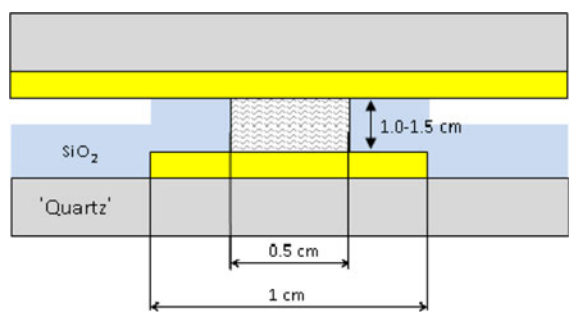

Fig. 2 GCM-1 silicon dioxide gap control method

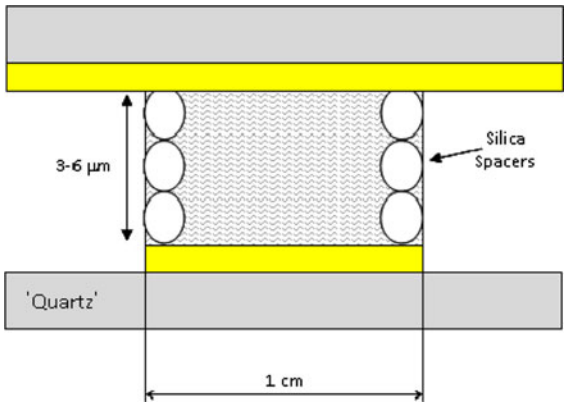

Fig. 3 GCM-2 silica particle gap control method

The first two methods of electrode spacing potentially left wide areas (~0.5–1.0 cm) of the electrodes unsupported, or supported only at the edges. In order to evaluate if flexing of the electrode plates was a factor, polymer pillar supports were fabricated across the electrodes (GCM-3). Photoresist pillars were made with Futerrex NR7-1500P resist spun at 3000 rpm for 40 s to produce 1.5 µm tall features with a diameter of 150 µm and pitch of 2.5 mm across the wafer surface. The pillars occupied a very small area so that the conduction area in these experiments remained essentially 1 cm^2 (Fig. 4).

A final experimental design involved the fabrication of comb electrodes with controlled gap size between the fingers of the comb. This test setup eliminated the possibility of mechanical shorting between the electrodes due to flexing of the parallel plates. It also allowed visual observation of the dielectric material without destroying the sample.

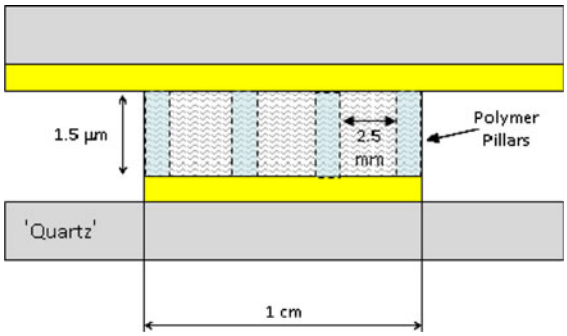

Fig. 4 GCM-3 polymer pillar gap control method

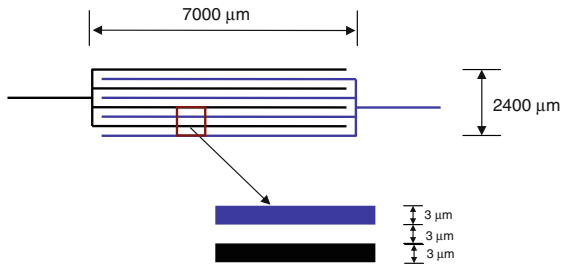

Fig. 5 Comb electrode schematic

A schematic of the comb geometry is shown in Fig. 5. The actual number of lines in the comb is 400, which is greater than what is shown conceptually in the diagram. The metal lines were fabricated from chromium metal and were 0.4 µm tall. The polymer materials were placed on the comb electrode surface with a dropper and exposed to 365 nm wavelength radiation under the same conditions as the parallel-plate samples.

For each experimental setup, after assembly, a voltage (e.g., 1 V) was applied across the electrodes with a precision, low-voltage power supply and the resistance between the capacitor plates was periodically measured with a volt meter. This voltage was maintained over the electrodes for up to 1 month. Each capacitor was connected in series with a 100,000 Ω resistor in order to limit the current to 10 µA, when conduction between electrodes occurred. After electrical measurements the electrodes were carefully inspected with an optical microscope. No protrusions, indentations or other visible surface alterations were found.

Results

The experimental results listed in Table 1 are presented in this section. These experiments focus on the POMA materials, comparing results with each of the gap control methods and the comb electrode experimental setup. In some of the experiments, electrode-to-electrode conduction was observed, when such conduction occurred, the minimum resistance across the electrodes was measured and is recorded in Table 1.

The POMA material was tested with a series of gap control methods and electrode materials. Two sets of gold parallel-plate electrodes were fabricated

Table 1 Summary of experimental results

Gap control method	GCM-1	GCM-2a	GCM-2a	GCM-2b	GCM-2b	GCM-3	Comb
Polymer	PDMS-1	PDMS-2	POMA	POMA	POMA	POMA	POMA
Polymer thickness (μm)	1–1.5	3–6	3–6	3–6	3–6	1.5	3
Electrode metal	Au	Au	Au	Au	Cr	Au	Cr
Metal thickness (μm)	0.5	0.5	0.5	0.5	0.5	0.5	0.4
Conduction area (cm^2)	0.25	1	1	1	1	1	0.01
R_{off} (Ω)	$>10^9$	$>10^9$	$>10^9$	$>10^9$	$>10^9$	$>10^9$	$>10^9$
R_{on} min (Ω)	1.10	3.45	1.00	1.20	47	$>10^9$	$>10^9$
% of Electrodes conducting	17	14	57	57	25	0	0

and tested with POMA using silica spheres as spacers. One set used silica spacers only in the corners of the electrode (GCM-2a) and the second set used spacers in the corners and in the center of the capacitor pads. In each case, there were seven independent electrodes (two electrodes were shorts before voltage was applied). In the first test (spacers on corners only), 4 of the 7 electrodes became conductive with resistances ranging from 1.0 to 4.2 Ω. Each conductive electrode behaved as a simple ohmic resistor over the voltage range measured (power supply limit was 0.2 A). A representative I–V plot is shown in Fig. 6.

The second POMA sample, which used spacers in the electrode corners and center (GCM-2b), had 4 of 7 electrodes become conductive with resistances ranging from 1.2 to 3.7 Ω. The effect of manually extending the voltage range beyond 0.2 V did not materially impact the linearity of the resistance. In those cases, the maximum current which could pass through the electrodes was 1.8 A. The in-phase (often called 'real-part') of an impedance scan as a function of frequency is plotted in Fig. 7. The impedance behavior is ohmic with little contribution from a parallel capacitance pathway between the two plates. The increase in impedance at high frequency was an artifact of the probes and not a contribution from the POMA.

A third parallel-plate experiment used gold electrodes with a photoresist pattern on the gold (GCM-3). The experiment used the NR7 resist pillars for spacing with gold electrodes. The purpose of this test was to minimize the distance between pillars to help ensure that mechanical shorting would not occur between the top and bottom electrodes while keeping a large portion of the electrode surface free for conduction. In this test, POMA was UV exposed using the standard conditions and eight electrodes were biased at 1 V. After 12 days, no conductivity was observed in any of the electrodes. Similar experiments were conducted with the PDMS materials and patterned silicon dioxide (GCM-1) on gold electrodes. The results were comparable to those with POMA, with a small number of tested electrodes

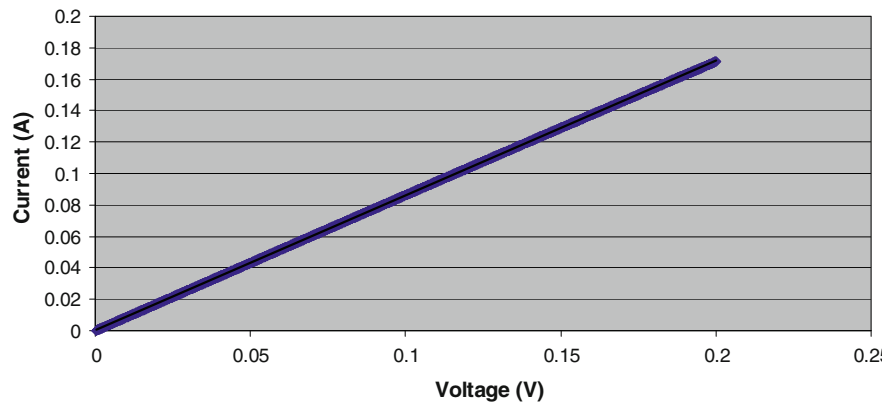

Fig. 6 I–V plot for POMA. $R = 1.24$ Ω

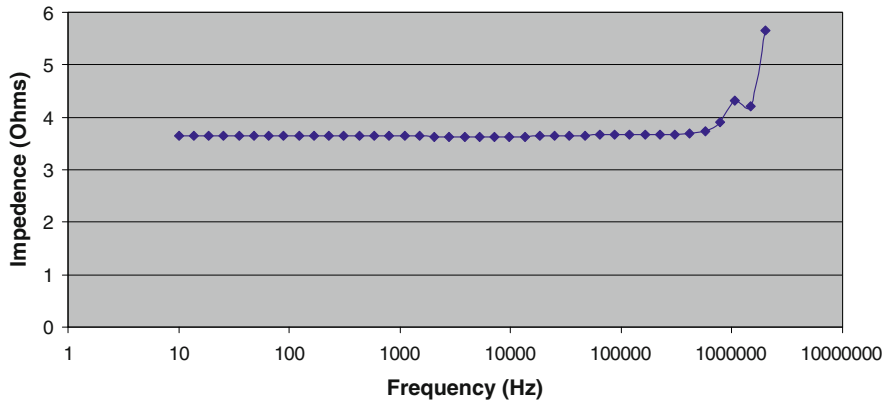

Fig. 7 Real part of the complex impedance for electrode *G* as a function of frequency

becoming conductive upon testing. These results are included in Table 1 but are not discussed in further detail here since the PDMS materials were not tested with the comb electrodes.

The fourth, and final, parallel-plate experiment utilized POMA with chromium electrodes and silica particles to control the gap spacing (GCM-2b). In this experiment both the bottom (patterned) and top electrodes were fabricated with chromium to replicate the materials used in the comb electrodes, which were fabricated with chromium and not gold. Four parallel-plate chromium electrodes were tested and one became conductive under bias. The resistance of this electrode dropped to a minimum of 47 Ω, higher than the samples with gold electrodes. This high resistance value is likely due to the higher resistivity of the chromium electrodes, as compared to gold, as well as the presence of chromium oxide and not to any changes in the polymer conduction mechanism.

Following the electrical testing, the top and bottom electrode from each capacitor tested were taken apart and inspected optically for any sign of defects formed on the electrode surfaces or in the polymer materials. The optical inspection was performed in a variety of microscopes at magnifications from 50× to 500×. The inspection of the polymer materials was difficult as the surface created on separating the plates was rough and the separation process itself could damage any conducting pathway present in the polymer. Thus, optical inspection did not reveal any noticeable features in the tested polymer materials, and optical images of this material are not included in these results. SEM and TEM analysis of any possible conducting layer was not feasible as the generally insulating polymer would not enable any observation below the surface, thus no such images are included in the analysis. Following this inspection the polymer was removed with acetone and the electrode surfaces were inspected in detail for defects. In each case there were no noticeable defects found on the metal electrode surfaces.

In addition to the parallel-plate experiments a number of comb electrodes were fabricated and tested with the POMA materials as the dielectric. The purpose of this experiment was to eliminate the possibility that electrodes could mechanically deform and short together to create the low-resistance measurements seen in the parallel-plate experiments. The comb design creates a rigidly set gap of 3 μm between electrodes as shown in Fig. 5, while also providing optical access to inspect the polymer in the case of conductivity. Twenty-seven comb electrodes were fabricated with chromium electrodes and tested with the POMA material, and the results are summarized in Table 2. The conductance between isolated combs was measured before and after UV exposure. It was found that the conductance consistently increased by a factor of ten following UV exposure, however, the value remained very small in all cases (i.e., <0.03 μS). Table 3 provides the conductance values measured before and after UV exposure for five of the tested comb electrodes.

Each comb electrode was initially biased at 1 V and with the voltage being increased eventually to a final voltage between 3 and 10 V for a total bias time of up to 25 days at similar electric field strength (V/cm) to the parallel-plate capacitors. There were no instances of conduction observed with the comb electrodes. Optical inspection showed no pitting,

Table 2 Comb electrode experimental results

Electrode	Time under voltage (days)	Voltage step applied (V)	Time of voltage step (days)	Conductivity observed
1	25	5 V then 10 V	7 and 10 days	No
2	25	5 V then 10 V	7 and 10 days	No
3	25	3	18	No
4	25	3	18	No
5	25	3	11	No
6	14	3	11	No
7	14	3	11	No
8	14	3	11	No
9	14	3	11	No
10	14	3	11	No
11	14	3	11	No
12	14	3	11	No
13	14	3	11	No
14	14	3	11	No
15	14	3	11	No
16	14	3	11	No
17	14	3	11	No
18	11	3	7	No
19	11	3	7	No
20	11	3	7	No
21	11	3	7	No
22	11	3	7	No
23	11	3	7	No
24	11	3	7	No
25	11	3	7	No
26	11	3	7	No
27	11	3	7	No

Table 3 Comb electrode conductance

Electrode	Conductance before exposure (μS)	Conductance after exposure (μS)
3	0.002	0.018
4	0.0022	0.0206
5	0.0025	0.017
6	0.003	0.021
7	0.003	0.0185

plating, or deformation of the lines after these tests and as there was no conduction there was no opportunity to observe conduction pathways in the polymer.

Discussion

The appearance of a conductance between two metal electrodes 1 and 2 separated by a normally insulating material implies formation of a 'bridge' of finite resistance R_{12} between the electrodes 1 and 2 (Fig. 8). The following possible 'bridge' cases will be considered:

(1) Metal filament originated from the electrodes
(2) Carbon filament originated from the polymer
(3) Direct contact between the electrodes 1 and 2 due to mechanical deformation
(4) Formation of a highly conductive region of unknown nature

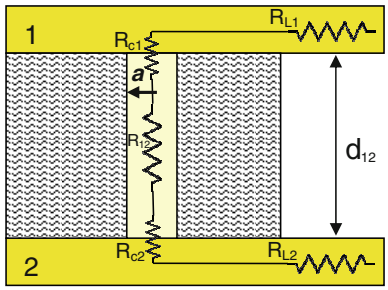

Fig. 8 Electrical schematic for the test cell

In all cases, the total measured resistance is a sum of four components (Fig. 8):

$$R_{\text{total}} = R_{\text{L1}} + R_{\text{L2}} + R_{\text{C1}} + R_{\text{C2}} + R_{12} \quad (1)$$

where R_{12} is the resistance of the 'bridge'; R_{C1}, R_{C2} are the constriction resistances of a contact between the bridge resistor and the electrodes; and R_{L1}, R_{L2} are the lead resistances.

The lead resistance R_{L1} is the resistance of a thin-film metal strip of length L, width W, and thickness t:

$$R_{\text{L1}} = \rho_{\text{Me}} \frac{L}{Wt} \quad (2)$$

The lead resistance R_{L2}:

$$R_{\text{L2}} = \frac{\rho_{\text{Me}}}{2\pi \cdot t} \quad (3)$$

Table 4 summarizes the parameters of the lead resistance. As follows from the Table 3, the lead resistance is close or within the measured range of HCP resistances in experiments 1, 3, and 4. Therefore, the interelectrode 'bridge' resistance R_{12} is small for these cases and t. The lead resistance can be eliminated by using 4-wire resistance measurement method, but this was not done in our experiments.

Scenario I: metal filament originated from the electrode

Consider a metal filament of radius a and length d_{12} that connects the electrodes 1 and 2. The filament resistance would be:

Table 5 Estimated values for contact and filament resistance for different filament diameters δ

δ (μm)	$R_{\text{C}} = (R_{\text{C1}} + R_{\text{C2}})$ (Ω)	R_{12} (Ω)	$R_{12} + R_{\text{C}}$ (Ω)
1.0	0.05	0.06	0.11
0.8	0.06	0.10	0.16
0.6	0.08	0.17	0.25
0.4	0.12	0.38	0.50
0.2	0.24	1.53	1.77
0.1	0.48	6.11	6.59

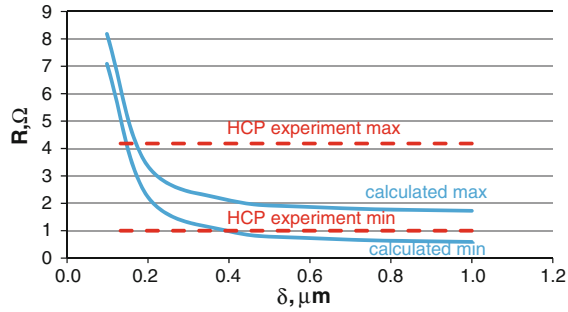

Fig. 9 Metal filament hypothesis: Calculated and experimental margins for total measured resistance

$$R_{12} = \rho_{\text{Me}} \frac{d_{12}}{\pi \cdot a^2} \quad (4)$$

Next, the constriction resistance (Jansen et al. 1980; Norberg et al. 2006) exists at points of contact between the filament and the electrodes 1 and 2:

$$R_{\text{C1}} = R_{\text{C2}} = \frac{\rho_{\text{Me}}}{2a} \quad (5)$$

The values of the contact and filament resistance for different diameters $\delta = 2a$ of the hypothetical gold filaments are shown in Table 5.

The total expected resistance R_{total} can be calculated from (1) and it is plotted in Fig. 9 for different filament diameters, δ. The max and min range of experimental results are also shown in the plot. Note the metal filament hypothesis requires the filament diameter of 0.2 μm or larger in order to be consistent with experimental data.

Table 4 Summary of calculated resistances for the test configuration

Me	ρ_{Me} (μΩ cm)	W_{L1} (mm)	L_{L1} (cm)	t_{L1} (nm)	t_{L2} (nm)	R_{L1} (Ω)	R_{L2} (Ω)	$R_{\text{L1}} + R_{\text{L2}}$ (Ω)
Au	2.4	1.5	1.5–5	500	500	0.48–1.60	0.008	0.49–1.61

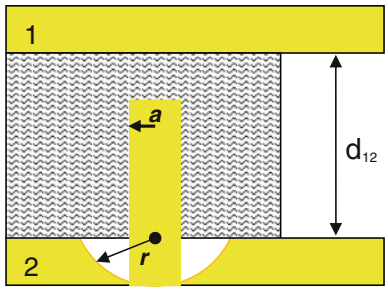

Fig. 10 Illustration to metal filament formation

We now estimate the mass transfer needed for the growth of metal filament. The volume of the filament v is:

$$v = \pi a^2 \cdot d_{12} \tag{6}$$

Since the filament originates from the electrode in this scenario, an equal amount of gold atoms should leave the surface of the electrode(s), thus forming a void 'crater' around the filament (Fig. 10).

Assuming a hemispherical shape of the crater (condition of equal travel distance for atoms), one can estimate the radius R of the crater

$$\frac{2}{3}\pi \cdot r^3 = \pi \cdot a^2 \cdot d_{12} \tag{7a}$$

or

$$r = \left(\frac{3}{2}a^2 d_{12}\right)^{\frac{1}{3}} \tag{7b}$$

Figure 11 shows the expected crater diameter $D_{\text{crater}} = 2r$ as a function of measured resistance. The crater diameters corresponding to the experimental resistance data are in the ~1–2 μm range. Observation using a microscope after completion of the experiment revealed no electrode pitting.

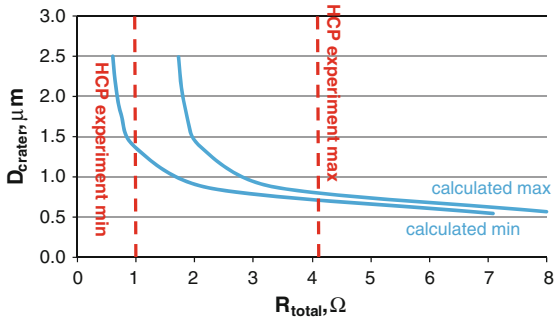

Fig. 11 Metal filament hypothesis: Crater diameter as a function of resistance

Scenario II: carbon filament originated from the polymer

There is a possibility of formation of carbon particles as result of partial decomposition of the polymer by the UV treatment. In principle, these carbon particles could migrate under the electric field and form a conductive pathway. Such a system resembles conductive composites, consisting of conductive filler powder dispersed in an insulating polymer matrix (Ruschau et al. 1992). Such conductive composites are commonly used in electronic applications, e.g., for die attach, thermistors, pressure sensing elements, etc., and an extensive literature exists on this topic.

For a numerical example in our study, data for polyethylene filled with carbon black at 30 vol.% loading was used (Ruschau et al. 1992). The reported resistivity of such a composite is 2 Ωcm (Ruschau et al. 1992).

Using this number, and repeating the calculations (4) and (5) for a filament resistance $R < 1\ \Omega$, a filament diameter $\delta > 220\ \mu\text{m}$ is obtained. Such agglomerations should be clearly visible with naked eye. Unfortunately, with the exception of the comb structures for which high conduction was not observed, it was not possible to observe the conduction pathways.

Scenario III: plate deformation

Consider a thin plate in the x–y plane in the region $x\ \varepsilon\ [0, a]$ and $y\ \varepsilon\ [0, b]$. We assume that the plate is thin relative to its dimensions with thickness h. Let p_z denote the pressure per unit area applied to the plate in the z direction. Then the differential equation describing small deformations in the z direction, say w, is given by:

$$D\nabla^4 w = p_z, \quad \text{or}$$
$$\frac{\partial^4 w}{\partial x^4} + 2\frac{\partial^4 w}{\partial x^2 \partial y^2} + \frac{\partial 4 w}{\partial y^4} = \frac{p_z}{D} \tag{8}$$

If it is assumed that the thin plate is simply supported around its boundary, then the boundary conditions are:

$$w = 0,$$
$$\frac{\partial^2 w}{\partial n^2} = 0,\ \forall (x, y)\varepsilon \text{ edge, and } n \text{ is the surface normal at the edge} \tag{9}$$

The constant D is given by:

$$D = \frac{Eh^3}{12(1-\nu^2)}, \tag{10}$$

where E is Young's Modulus, h is the material thickness, and ν is Poisson's Ratio. The following parameters for silicon were used in the numerical analysis: $E = 1.50 \times 10^{11}$ N/m^2, $\nu = 0.25$, and $h = 0.625 \times 10^{-3}$ m. Also, $a = 5 \times 10^{-3}$ m and $b = 5 \times 10^{-3}$ m were used for the size of the polymer container. In general, (8) is difficult to solve and numerical methods are normally used. However, for a simple unsupported plate (not clamped) at constant pressure, p_z, a series solution can be given (Eq. 11).

$$w(x,y) = \sum_m \sum_n \frac{16p_0 \sin(m\pi x/a)\sin(n\pi y/b)}{(\pi^2 mnD)[(m\pi/a)^2 + (n\pi/b)^2]^2} \tag{11}$$

This expression was evaluated at $x = 2.5 \times 10^{-3}$ m and $y = 2.5 \times 10^{-3}$ m (the center of the thin plate). The summation converged when six terms were used for the x and y summations. The result was:

$$\frac{w(.5a,.5b)}{p_0} \approx 1.17 \times 10^{-12} \tag{12}$$

The density of silicon is approximately 2330 kg/m^3 and the total force acting, due to gravity, on the 5×5 mm plate is calculated from $F = ma = 15.625 \times 10^{-9}$ m^3 $\times$ 2330 $\times$ 9.8 $= 5.7085 \times 10^{-4}$ N. For reference, the effective gravitational pressure is $F/A = 5.7085 \times 10^{-4}/25 \times 10^{-6} = 14.72$ N/m^2. Thus from Eq. 5, the estimated deflection at the plate midpoint due to gravity is

$$\begin{aligned} W(.5a,.5b) &= 1.17 \times 10^{-12} \times 14.72 \\ &= 16.7 \times 10^{-12} \text{ m } (\text{or } 16.7 \times 10^{-6}\mu\text{m}). \end{aligned} \tag{13}$$

The pressure that would need to be applied uniformly across the plate to achieve a deflection of 1 μm can be estimated from the above data. Specifically,

$$P_{1\,\mu m} = 10^{-6}/1.17 \times 10^{-12} = 0.85 \times 10^6 \text{ N/m}^2 \tag{14}$$

This is below the fracture limit for bulk silicon which is approximately 2.7×10^8 N/m^2. From Eq. 7, the effective force that would be required is $F_{\text{critical}} = P_{1\,\mu m} \times A = 21.25$ N. This would be equivalent to a 2.17 kg mass resting on the top plate. This value is consistent with simple experiments performed during capacitor setup where the two plates were squeezed by hand and tested for shorting. After assembly of the capacitors with the dielectric material in place, some of the structures were squeezed by hand (thumb and forefinger). Shorting of the plates was often observed. While the forces were not quantified, the values were consistent with the estimation given above.

The electrostatic pressure between parallel electrodes is approximately:

$$P_E = \frac{k\varepsilon_0 v^2}{2d^2} = 4.43k \text{ N/m}^2 \tag{15}$$

For values of k in the range of 3, this pressure is approximately the same as the effective pressure due to gravitational forces acting on the upper electrode plate and hence the deflection of the plate would be negligible.

An electrostatic force, F_e, results from the potential difference applied across the two capacitor plates (Chinthakindi and Kohl 2002). For example, if a movable plate of area A is separated from an immovable plate by distance d, then the electrostatic force is given by Eq. 16.

$$F_e = \varepsilon_0 AV^2/2(d-x)^2 \tag{16}$$

where x is the deflection from the starting displace d, V is the applied voltage, and ε_0 is the permittivity of free space. If the movable plate were restrained by a simple spring whose restraining force is equal to kx, where k is a spring constant, then the point of mechanical instability occurs at a deflection of $x = d/3$. That is, once the upper plate moves a distance $d/3$, the two plates snap together because the electrostatic force (proportional to $1/(d-x)^2$) exceeds the mechanical restoring force.

In the case of the parallel-plate electrodes constructed here, the top plate is restrained by a simple spring. Estimates of the restraining force for the deflection of the top plate shows that the applied voltage is not sufficient to cause mechanical instability, for a defect free dielectric material held within a uniform capacitor gap. One would need to have either a thinner gap or higher dielectric constant (e.g., caused by defects) within the dielectric material separating the plates. However, the required applied voltage or size and nature of the defects so as to cause

mechanical instability is not so excessive so as to exclude this possibility given the nature of the materials and processing conditions, such as excessive UV exposure.

Scenario IV: formation of a highly conductive region of unknown nature

Assume that the HCP hypothesis is correct and that a highly conductive region ('bridge') with $R_{12} = 0$ was formed between the metal electrodes. Even for zero 'bridge' resistance R_{12}, the total measured resistance R_{total} would be greater than zero due to the constriction resistance (5) and the lead resistance (2) and (3). While the lead resistance could be eliminated by using a 4-wire measurement technique (see the next section), the constriction resistance sets a fundamental lower limit on R_{total}. From (5) and Table 4, if the 'bridge' diameter is less than 100 nm, the minimum measured resistance is larger than 0.5 Ω even in case of zero resistance of the 'bridge'.

The total HCP resistance R_{total} expected in these experiments it is plotted in Fig. 12 for different δ. The max and min range of experimental results are also shown in the plot. Note that if the 'filament' diameter is 100 nm or smaller, the HCP hypothesis is consistent with experimental data.

In some of the experiments outlined above, an increase in conductance was observed. The change in conductance appears consistent with previous literature reports where a low-voltage potential difference results in an increase in conductance (ca. ohm resistance) in some of the samples. It seems that there are several potential explanations for this behavior which can be considered. Possible explanations for the observed data are stated as hypotheses and the pros and cons of the explanation are discussed.

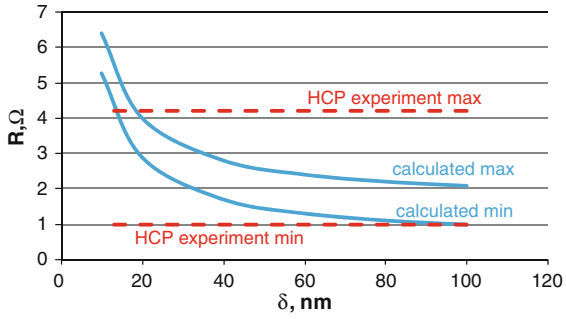

Fig. 12 HCP hypothesis: Calculated and experimental margins for total measured resistance

Hypothesis 1 The observed conduction was due to the formation of metal filaments between upper and lower electrodes

Pros: The formation of metal filaments can happen especially when copper or other less noble metals are used. A 1 V potential difference is sufficient to oxidize copper at the positive electrode, transport the ions to the negative electrode and redeposit the metal in the form of a nodule. In fact, preliminary experiments in this study (not reported here) used copper electrodes. Pitting and nodule formation was observed along with conduction. Since the source of the conduction was identified as metallic nodules, all copper experiments were terminated.

Cons: The gold and chromium electrodes underwent 100% microscopic inspection for nodules. No nodules were found. Further, a potential difference of 1 V is not sufficient to oxidize and redeposit gold in this electrolyte. Chromium forms a protective oxide and does not easily redeposit in nodule form. In our opinion, the formation of metal filaments as the source of conduction is exceedingly unlikely. This view is supported by the analysis offered in Scenario I.

Hypothesis 2 The observed conduction resulted from deformation of the electrode plates in such a way that contact was established

Pros: Thin, flat silicon or glass plates can bend and bridge the gap between the two electrodes under the electrostatic force and mechanical instability criteria, Eq. 16. The small area contact that would form from a bowed plate would have limited contact area resulting in modest conduction. These observations are consistent with limited contact area. The resistance was never below the ohm range. If the conduction area was 1 cm^2, one would observe resistance values orders of magnitude lower for a metal electrode. For example, mechanical electrical connectors often have resistances in the milli-ohm range. Further, no conduction was observed with rigid or non-flexing configurations. It should be noted that all the dielectrics exhibiting this form of conduction are viscous liquids which could facilitate deformation of the plates. Further, the assistance or need for the extremely high dose of UV radiation and

time delay is curious. This level of exposure can cause normally unlikely photochemical reactions, which do not occur in high purity electronics grade dielectrics. Identification of such reactants and products would be a very difficult analytical task.

Cons: The field applied was less than the critical mechanical instability point for electrostatic attraction and 'snap-down' of two metal plates. That is, the electrostatic force was less than that needed to cause mechanical closure of the gap. However, the exceedingly high UV exposure and long bias time prior to conduction provide ample time and energy for the creation and/or growth of particles and impurities which can partially or fully bridge the gap between the two electrodes. All of the dielectrics used in these and previous studies contain unknown purities, moisture, and residual solvent. It is noted that identification and isolation of particles is very difficult because each sample had to be nearly destroyed after testing in order to recover the dielectric. Moreover, the analysis offered in section Scenario III suggests that electrostatic and gravitational forces would be unlikely to deform the plates sufficiently to achieve electrode contact. A substantial external force would be necessary to achieve partial contact.

Hypothesis 3 The polymers actually transitioned into a highly electrically conductive mode

Pros: Conduction does occur and process is reproducible. Without identification of a viable metallic pathway, such as in Hypothesis 2, one is faced with explaining the formation of a highly conductive pathway in a non-conductor at potential far below the dielectric breakdown voltage.

Cons: No conduction was observed with fixed electrodes.

Conclusion

In some of the configurations tested, highly conductive phenomena were sometimes observed after UV irradiation and applying a voltage of 1 V for extended periods of time. Analyses of the data obtained in these cases are consistent with the hypothesis that a highly conducted pathway was formed. These analyses suggest that metal filament formation between the electrodes is unlikely and that carbon pathways formed from polymer impurities would have been quite visible. Unfortunately, the structure of the experimental apparatus in the cases where high conductance was observed did not submit to visual inspection. Moreover, unless the electrodes were badly misaligned from a parallel configuration, plate bending analyses indicate that bending due to gravitational and electrostatic pressures to achieve electrode contact is unlikely.

On the other hand, no conduction was observed for the comb electrode test apparatus where visual inspection allowed us to confirm that the integrity of electrode separation was maintained. There is a room for skepticism regarding the hypothesis that polymers, under the conditions of irradiation and embedding in a low electric field for an extended period of time can become highly conductive. Nevertheless, the data we have obtained and our analyses do not allow us to rule this possibility out. We believe that additional experiments might allow a more definitive conclusion. Specifically, the test apparatus should be designed so that potential conduction pathways are available for inspection at all times. Secondly, electrical measurements should use the 4-wire technique to eliminate resistance contributions of external leads and contacts.

Acknowledgment The authors wish to acknowledge the support and advice of Dr. Kevin Shambrook (Physics Faculty, Diablo Valley College, CA; kevin.shambrook@gmail.com) in the conduct of this study.

References

Chinthakindi A, Kohl PA (2002) Electrostatic actuators with intrinsic stress gradient—II. Performance and modeling. J Electrochem Soc 149:H146

Enikolopyan NS et al (1989) Possible Superconductivity near 300-K in oxidized polypropylene. JETP Lett 49:371–375

Ionov AN et al (1992) Low-resistance state in polydipheylenephthalide at low temperature. Solid State Commun 82:609

Ionov AN et al (2005) High conductivity and supercurrent in superconductor-polymer-superconductor systems. Phys B 359:506

Ionov AN et al (2007) Local distribution of high-conductivity regions in polyamide thin films. JEPT Lett 85:636

Jansen AGM et al (1980) Point-contact spectroscopy of metals. J Phys C 13:6073

Norberg G et al (2006) Contact resistance of thin metal film contacts. IEEE Trans Compon Packag Technol 29:371

Rogachev DN, Grigorov LN (2000) Observation of extremely large, field-dependent diamagnetism at 300 K in certain disordered organic materials. J Supercond Novel Magn 13:947

Ruschau GR et al (1992) Resistivities of conductive composites. J Appl Phys 72:953

Shlimak I, Martchenkov V (1998) Switching phenomena in elastic polymer films. Solid State Commun 107:443–446